Rare Metal Materials and Engineering
Volume 52, Issue 1, January 2023
Available online at www.rmme.ac.cn

Science Press

Cite this article as: Zhao Meili, Gan Guoyou, Leng Chongyan, et al. Synthesis Mechanism and Deformation Mechanism of Silver Nanowires with Different Aspect Ratios[J]. Rare Metal Materials and Engineering, 2023, 52(01): 6-14.

ARTICLE

Synthesis Mechanism and Deformation Mechanism of Silver Nanowires with Different Aspect Ratios

Zhao Meili[1], Gan Guoyou[1], Leng Chongyan[1], Xu Fengxian[1], Yuan Peng[1], Bai Hailong[2], Lv Jinmei[3], Yan Jikang[1,4]

[1] Faculty of Materials Science and Engineering, Kunming University of Science and Technology, Kunming 650093, China; [2] R&D Center, Yunnan Tin Group (Holding) Co., Ltd, Kunming 650000, China; [3] Yunnan Tin Industry Tin Material Co., Ltd, Kunming 650501, China; [4] School of Engineering, Southwest Petroleum University, Nanchong 637001, China

Abstract: Silver nanowires with different aspect ratios were prepared by adjusting the molar content of polyvinylpyrrolidone (PVP) through the liquid-phase reduction method. X-ray diffractometer, scanning electron microscope, UV-Vis spectrophotometer, simultaneous thermal analyzer, and transmission electron microscope were used to characterize the phase composition, microstructure, light absorption properties, thermal decomposition, and crystal structures of the silver nanowires, and the molecular dynamics was used to simulate the stretching and melting processes of single-crystal silver nanowires. Result shows that the silver nanowires are mainly composed of face-centered cubic silver. When the molar ratio of PVP to $AgNO_3$ changes from 1.5 to 7.5, the diameter of silver nanowires firstly decreases and then increases, and the minimum diameter of nanowires is 77.7 nm when the molar ratio is 6.0. With decreasing the diameter of silver nanowires from 106.1 nm to 77.7 nm, the melting temperature is decreased, and the lowest melting temperature is 281.2 °C. The yield strength is gradually increased from 0.63 GPa to 0.83 GPa with increasing the aspect ratios of silver nanowires from 6 to 72. The melting temperature of single-crystal silver nanowires is decreased from 690 K to 657 K with increasing the aspect ratio. Therefore, the molar ratio of 6.0 is the optimal condition to synthesize silver nanowires, and the silver nanowires with a large aspect ratio have good resistance to deformation.

Key words: liquid-phase reduction; silver nanowires; growth mechanism; molecular dynamics; aspect ratio

Silver nanowires are one-dimensional materials with transverse length limit of 100 nm and unlimited vertical length[1]. Due to their good electrical properties, excellent optical properties, and significant nanometer effects[2], silver nanowires are commonly used to prepare transparent conductive electrodes instead of InSnO materials. Many methods have been developed to prepare silver nanowires, such as crystal seed, template, and sol-gel methods[3–5]. Liu et al[6] used AgCl as the crystal seeds and found that the aspect ratio of the synthesized silver nanowires is more than 1000 when the molar ratio of AgCl to $AgNO_3$ is 1∶5. Sun et al[7] adopted the solvothermal method and found that the prepared silver nanowires have good crystallinity and their aspect ratio can reach 200 with low cost. Yuan et al[8] synthesized the silver nanowires at low temperatures with $AgNO_3$ as the starting agent and the dimethylformamide as solvent and reducer. The prepared silver nanowires have good uniformity and their length is up to 20 μm. Although the preparation and properties of silver nanowires have been widely researched, the formation mechanism of silver nanowires is rarely reported.

Molecular dynamics (MD) [9] is a simulation method to study the system equilibrium thermodynamics and structural dynamics. Recently, the deformation behavior of materials during stretching and melting by molecular dynamics has been widely researched. Zhang et al[10] simulated the unidirectional tensile process of Ti-Al nano-rods and found that the simulation results are consistent with the experimental

Received date: August 31, 2022
Foundation item: Innovation Team in Yunnan Province (202105AE160028); Fundamental Research and Applied Basic Research Enterprise Joint Project Between Yunnan Provincial Department of Science and Technology and Yunnan Tin Group (Holding) Co., Ltd (202101BC070001-010)
Corresponding author: Yan Jikang, Ph. D., Professor, School of Engineering, Southwest Petroleum University, Nanchong 637001, P. R. China, E-mail: yanjk@swpu.edu.cn

ones. Wang et al[11] simulated the stretching process of silver nanowires with different twin densities and found that the twin boundaries can strengthen the nanowires. Zhao et al[12] simulated the stretching process of silver nanowires with diverse initial structures and found that the defects and twin crystals can cause stress concentration.

In this research, the polyol reduction method[13–14] was used, polyvinylpyrrolidone (PVP) of different molar contents was added to prepare the silver nanowires with different aspect ratios, and the mechanism of lateral growth inhibition of silver nanowires by PVP was investigated. The deformation behavior of monocrystal silver nanowires during stretching and melting was analyzed by MD method. The results provided research basis for the investigation of failure mechanism of flexible transparent conductive films.

1 Experiment

$AgNO_3$, PVP, NaCl, and KBr were dissolved in ethylene glycol to obtain Solution A, Solution B, Solution C, and Solution D, respectively. Solution B was heated continuously at 170 °C for 90 min and then cooled down to 160 °C. Solution C of 2 mL and Solution D of 1 mL were added to Solution B and then heated for 15 min. Solution A was added to the mixed solution at titration rate of 1 mL/min and then heated for 60 min. The mixed solution gradually changed from transparent yellowish liquid to white opaque, and gray flocculent materials were produced to obtain silver products of different structures.

Finally, an appropriate amount of anhydrous ethanol was added to the reaction solution and centrifuged at 2000 r/min for 5 min. The supernatant was poured off. The lower precipitate was dispersed in anhydrous ethanol and washed by anhydrous ethanol or deionized water for 3 or 4 times to obtain the pure silver nanowires.

D8-ADVANCE X-ray diffractometer (XRD) was used to analyze the phase composition. UV-5900PC UV-visible spectrophotometer (UV-Vis) was used to analyze the light absorption properties of the silver nanowires. The microstructure and crystal structure of silver nanowires were observed by HITACHI SU8010 cold-field scanning electron microscope (SEM) and TecniaG2 TF30 S-Twin transmission electron microscope (TEM). The thermal decomposition properties of silver nanowires were analyzed by NETZCH STA449F3 synchronous thermal analyzer.

2 Results and Discussion

2.1 Effect of PVP/$AgNO_3$ on silver nanowires

2.1.1 Phase analysis

Fig.1 shows XRD patterns of the silver nanowires prepared with different PVP/$AgNO_3$ molar ratios. According to Fig. 1, the sharp diffraction peaks appear around 2θ=38°, 44°, 64°, and 77°, which correspond to the (111), (200), (220), and (311) crystal planes, respectively, indicating the face-centered cubic (fcc) silver. Therefore, the silver nanowires are mainly composed of fcc silver with good crystallinity. In addition,

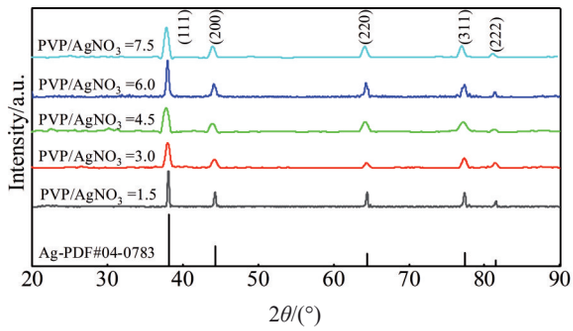

Fig.1 XRD patterns of silver nanowires with different PVP/$AgNO_3$ molar ratios

when the molar ratio of PVP/$AgNO_3$=1.5, the ratio of peak intensity of (111) plane to peak intensity of (200) plane $I_{(111)}/I_{(200)}$=2.5; when PVP/$AgNO_3$=3.0, $I_{(111)}/I_{(200)}$=2.9; when PVP/$AgNO_3$=4.5, $I_{(111)}/I_{(200)}$=3.0; when PVP/$AgNO_3$=6.0, $I_{(111)}/I_{(200)}$=3.4; when PVP/$AgNO_3$=7.5, $I_{(111)}/I_{(200)}$=2.8. The experimental result of $I_{(111)}/I_{(200)}$ with PVP/$AgNO_3$=1.5 is equal to the theoretical value of $I_{(111)}/I_{(200)}$ with PVP/$AgNO_3$=2.5, because the main product is silver nanoparticles and the silver nanowires are of low purity, which is consistent with the result in Fig. 2. The experimental results of $I_{(111)}/I_{(200)}$ with PVP/$AgNO_3$=3.0, 4.5, 6.0, and 7.5 are higher than the theoretical values due to the increased content of silver nanowires and the selective growth of nanowires along the (111) crystal plane.

2.1.2 UV-Vis analysis

Fig. 3 shows UV-Vis spectra of silver nanowires with different PVP/$AgNO_3$ molar ratios. It is found that the silver nanowires with different molar ratios have different light absorption properties. A strong absorption peak appears at 438 nm when PVP/$AgNO_3$=1.5, which is the absorption peak corresponding to spherical silver nanoparticles caused by the nanoparticle dipole appearance resonance[15–16]. This phenomenon indicates that the main products are silver nanoparticles when PVP/$AgNO_3$=1.5. A strong absorption peak at 373 nm and a weak peak at 354 nm appear when PVP/$AgNO_3$=3.0, which are the typical absorption peaks of silver nanowires. Particularly, the occurrence of the absorption peak at 354 nm is due to the longitudinal plasmon resonance absorption of the

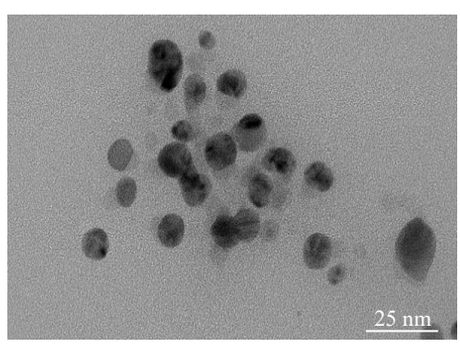

Fig.2 TEM morphology of silver nanowires with PVP/$AgNO_3$ molar ratio=1.5

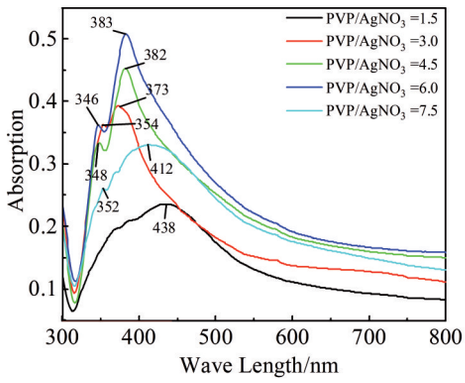

Fig.3 UV-Vis spectra of silver nanowires with different PVP/$AgNO_3$ molar ratios

silver nanowires, while the occurrence of the absorption peak at 373 nm is due to the transverse plasmon resonance[17]. When PVP/$AgNO_3$=4.5, the transverse surface plasmon resonance (SPR) peak of the silver nanowires undergoes obvious redshift to 382 nm, and the longitudinal SPR peak also suffers the redshift to 348 nm, indicating that the synthesized silver nanowires have high aspect ratio. When PVP/$AgNO_3$=6.0, the transverse SPR peak and the longitudinal SPR peak of the silver nanowires have slight redshifts and an increase in peak intensity, showing that the length of the silver nanowires increases. When PVP/$AgNO_3$=7.5, the transverse SPR peak undergoes the redshift to 412 nm, and the longitudinal SPR peak undergoes the redshift to 352 nm. Meanwhile, their peak intensities decrease, and the peak widths extend, indicating the increase in the diameter of silver nanowires.

2.1.3 Microstructure

PVP was used as surfactant during the growth of silver nanowires, which can selectively adsorb on different crystalline surfaces to control the aspect ratios of silver nanowires. Fig. 4 shows SEM morphologies of silver nanowires synthesized under different PVP/$AgNO_3$ conditions. The diameters of ten silver nanowires were measured, and the average diameter and variance were calculated, as shown in Fig. 5. The inhibitory effect on the lateral growth of silver nanowires is firstly strengthened and then weakened with increasing the PVP content. The most obvious inhibition effect on lateral growth occurs with PVP/$AgNO_3$=6.0. In conclusion, the morphology and aspect ratio of the silver nanowires can be controlled by adjusting the molar ratio of PVP to $AgNO_3$.

Fig. 6 shows TEM morphologies and selected area electron diffraction (SAED) pattern of silver nanowires with PVP/$AgNO_3$=6.0. According to Fig.6a, the aspect ratio of the silver nanowires with PVP/$AgNO_3$=6.0 is about 96. As shown in Fig.6b, PVP film is attached to the surface of silver nanowires, leading to the smoother and more uniform nanowire surface. In addition, the longitudinal side of the silver nanowires is connected by five (100) crystal planes[18–20], thus showing a pentagonal cross-section. Fig. 6c shows the high-resolution TEM microstructure of the silver nanowires with the Fourier transformed lattice image. It can be seen that the spacing of the crystal planes parallel to $[01\bar{1}]$ plane and the connecting twin grain boundaries is 0.2438 and 0.2000 nm, which are consistent with the spacing of (111) and (200) crystal planes of fcc silver, respectively. According to Fig.6d, more than two sets of diffraction patterns can be observed, and each set of diffraction spots can be assigned to the fcc crystal with the $[01\bar{1}]$ crystal band axis.

The surface energy can be calculated by Eq. (1)[21], as follows:

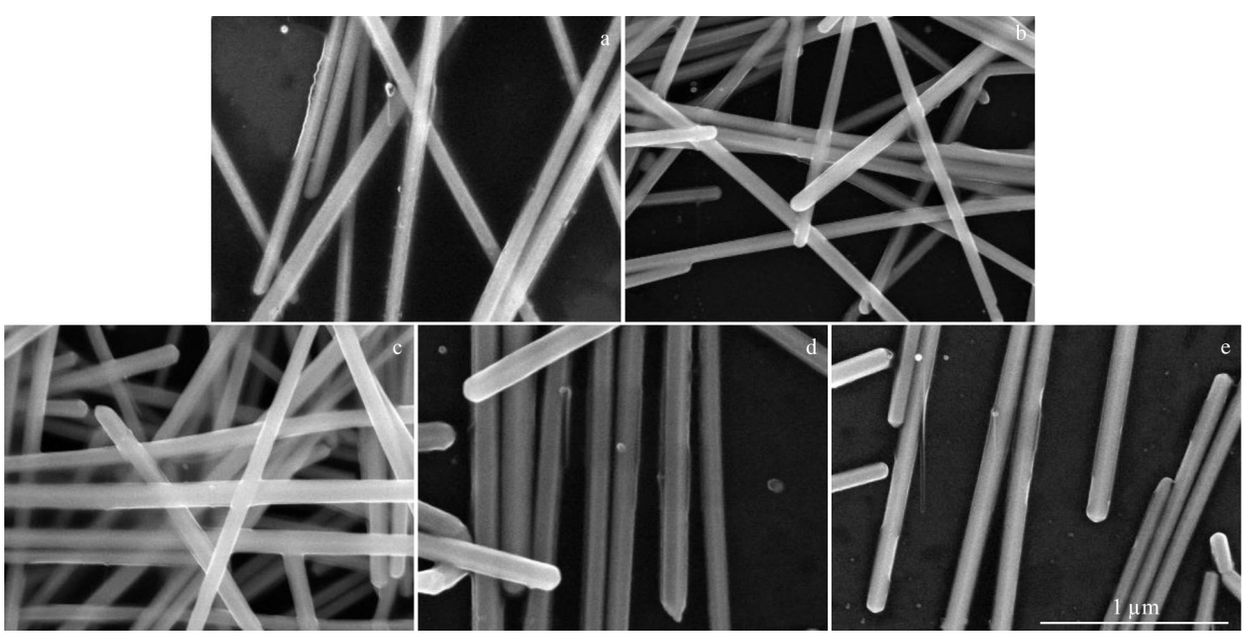

Fig.4 SEM morphologies of silver nanowires with different PVP/$AgNO_3$ molar ratios: (a) PVP/$AgNO_3$=1.5; (b) PVP/$AgNO_3$=3.0; (c) PVP/$AgNO_3$=4.5; (d) PVP/$AgNO_3$=6.0; (e) PVP/$AgNO_3$=7.5

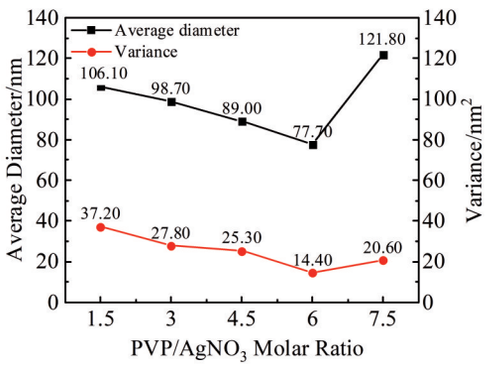

Fig.5 Average diameter and variance of silver nanowires with different PVP/$AgNO_3$ molar ratios

$$\gamma = \Delta E - T\Delta S \quad (1)$$

where γ is the surface energy (J/m^2); ΔE is the internal energy of the surface (J); $T\Delta S$ is the surface entropy (J/mol).

According to Fig. 6d, the crystalline planes of silver nanowires do not completely coincide with the densest (111) plane. The internal surface energy and the orientation difference angle can be expressed by Eq.(2)[22–23], as follows:

$$\Delta E = (\cos\theta + \sin\theta)\varepsilon/2a \quad (2)$$

where ΔE is the internal energy of the surface (J); $\sin\theta/a$ is the number of broken bonds in the vertical direction; $\cos\theta/a$ is the number of broken bonds in the horizontal direction; $\varepsilon/2$ is the bond energy provided by each broken bond (J).

When the system temperature is low, the surface entropy can be ignored, and the internal energy of the surface is regarded as the surface energy. When the system temperature is high, the surface entropy is positive, i. e., $\gamma < \Delta E$. The reaction temperature in this research is 160 °C, so the surface entropy cannot be neglected. The relationship between the surface energy and the orientation difference angle is shown in Fig. 7. When the Ag (111) crystal plane overlaps the densest plane, the misorientation angle is 0° . The misorientation angles of the densest plane with Ag (100), Ag (110), and Ag (311) crystal planes are 54.7°, 35.3°, and 29.5°, respectively. Therefore, the surface energies of different crystal planes are different: $\gamma_{(100)} > \gamma_{(110)} > \gamma_{(311)} > \gamma_{(111)}$. The Ag (111) crystal plane has the lowest surface energy, so the crystallization nuclei grow preferentially on the Ag (111) crystal plane to minimize the system energy. However, this spontaneous growth is very slow. Thus, PVP is added as a guiding agent to promote the crystal growth. PVP has different effects on different crystal planes. PVP has the most significant influence on the Ag (100) crystal plane: it firstly absorbs on Ag (100) crystal plane, passivates the crystal planes, reduces the surface energy, hinders the deposition of Ag atoms on the crystal planes, and inhibits the lateral growth of silver nanowires. PVP has the weakest inhibitory effect on the Ag (111) crystal plane: Ag atoms are deposited on the crystal plane for continuous anisotropic growth, and the one-dimensional silver nanowires are obtained. When PVP content is low, the inhibition of lateral growth is weakened, and the silver nanowires are coarsened. When PVP content is high, some Ag (111) crystal planes are passivated, and the aspect ratio of silver nanowires is reduced. As a result, the silver nanowires with different aspect ratios can be prepared by

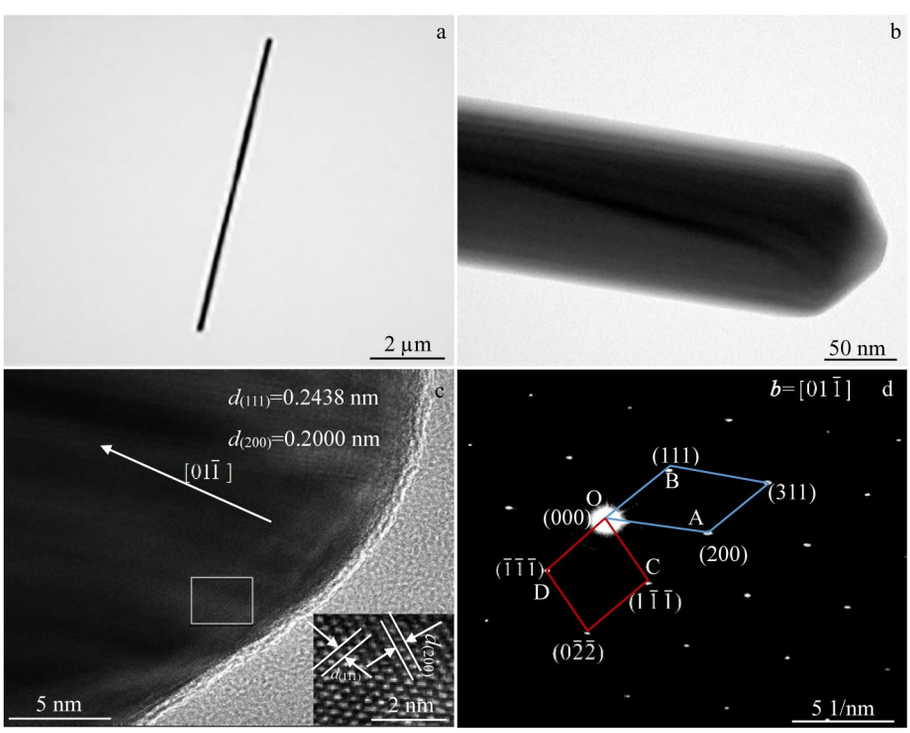

Fig.6 TEM morphologies of silver nanowires with PVP/$AgNO_3$=6.0: (a) overall nanowire, (b) nanowire end, and (c) high-resolution microstructure of nanowire end; SAED pattern of rectangular area in Fig.6c (d)

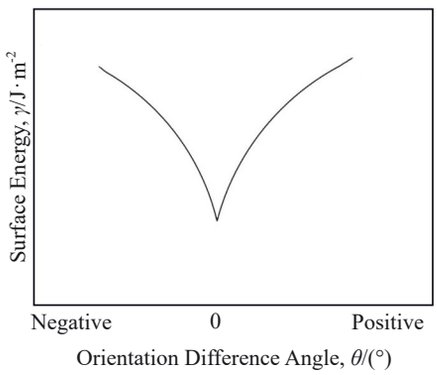

Fig.7 Relationship between surface energy and orientation difference angle

adjusting the PVP content.

2.1.4 Thermal analysis

Fig.8 shows the thermal analysis curves of silver nanowires with different PVP/$AgNO_3$ molar ratios at 40–900 °C. The protective gas was argon, and the heating rate was 10 °C/min. Table 1 shows the melting temperatures of the silver nanowires with different PVP/$AgNO_3$ molar ratios. Wen et al[24] reported that the silver nanowires firstly deviate from the equilibrium during the melting process and then the ordered structure is destroyed. When the temperature rises to a specific value, the nanowires break off and form nanoclusters. It can be seen from Table 1 that the melting temperature of silver nanowires is much lower than that of single-crystal silver. Besides, the melting temperature has the similar variation trend to that of the nanowire diameter: the melting temperature is firstly decreased and then increased, and the lowest melting temperature of nanowires is 281.2 ° C. Therefore, with increasing the nanowire diameter, the melting temperature is increased. The bonding energy of atoms is also improved with increasing the diameter of silver nanowires. Thus, the bulk melting of the nanowires occurs. Fig. 8 shows that when PVP/$AgNO_3$=1.5 and 7.5, two heat absorption peaks can be observed on the heat flow curves, which are caused by the insufficient purity of the silver nanowires and the existence of silver nanoparticles.

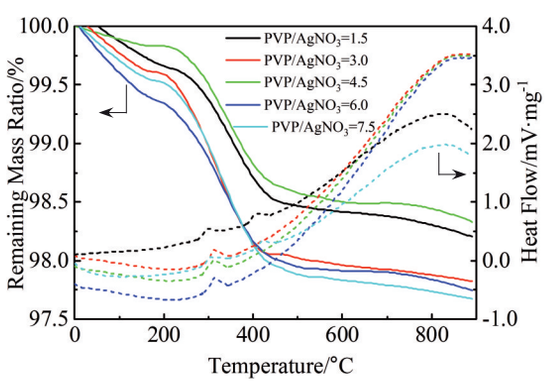

Fig.8 Thermal analysis curves of silver nanowires with different PVP/$AgNO_3$ molar ratios

Table 1 Melting temperatures of silver nanowires with different PVP/$AgNO_3$ molar ratios

PVP/$AgNO_3$ molar ratio	Melting temperature/°C
1.5	285.9
3.0	281.9
4.5	281.7
6.0	281.2
7.5	287.2

The thermogravimetric curves show that the maximum mass loss of the silver nanowires is 2.3% when PVP/$AgNO_3$= 7.5, and the thermal mass loss can be divided into three stages. The first stage of mass loss is at 280–290 °C, which corresponds to the decomposition of ethylene glycol and anhydrous ethanol. The second stage of mass loss occurs in the melting temperature range of the silver nanowires, where the fracture and decomposition appear. The third stage of mass loss occurs beyond 480 ° C, which is related to the PVP decomposition with the maximum mass loss of 0.65% under the condition of PVP/$AgNO_3$=3.0. Thus, it can be inferred that the silver nanowires are heavily encapsulated by PVP under the condition of PVP/$AgNO_3$=3.0.

2.2 Molecular dynamics calculations

2.2.1 Simulation method

The mechanical behavior and melting process of [110] - oriented single-crystal silver nanowires with different aspect ratios were studied. The initial structure is arranged according to the ideal fcc structure with a circular cross section, as shown in Fig. 9. To better simulate the natural system, the periodic boundary conditions were used along X and Z directions, and non-periodic boundary conditions were chosen along Y direction. The isobaric isothermal (NPT) system was used in this simulation. The interaction potential between atoms was described by the embedded atomic potential (EAM)[25], which involves the lattice parameters, elastic constant, and cohesion energy of Ag atoms. EAM (E_i) can be used to evaluate the structural stability of nanomaterials, and E_i is expressed by Eq.(3), as follows:

$$E_i = 1/2 \sum_{j,i} V_{ij}(r_{ij}) + F_i(\bar{\rho}_i) \quad (3)$$

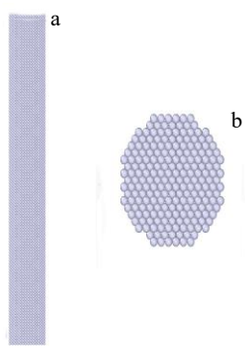

Fig.9 Schematic diagrams of initial model (a) and its cross section (b)

where $1/2\sum_{j,i}V_{ij}(r_{ij})$ is the interaction potential; r_{ij} is the spacing between atoms i and j; $F_i(\bar{\rho}_i)$ is the atomic cloud embedding energy determined by the average electron cloud density ρ_i at the atom location F_i. This potential function can simulate the multibody metal bonds by embedding atoms onto the lattice array as impurities.

2.2.2 Stretching process

Fig. 10a shows the stress-strain curves of silver nanowires with different aspect ratios (L/d) during the stretching process. It can be seen that the silver nanowires firstly enter into the elastic deformation stage during the stretching process, and the strain is increased linearly with increasing the stress until the yield point occurs. After the yield point, the silver nanowires enter into the plastic deformation stage. The stress of silver nanowires firstly decreases, then fluctuates periodically, and finally decreases due to the fracture. The fracture process of silver nanowires is shown in Fig.11.

In the elastic deformation process, the crystal structure is one of the main factors affecting the strength of materials. It can be seen from Fig. 10b that the increment in yield stress is reduced with increasing the aspect ratio of silver nanowires. The yield stress is 0.63 GPa when the aspect ratio L/d=12. The yield stress increases rapidly to 0.75 GPa when L/d=24. The yield stress is 0.80 GPa when L/d=48, and the increment in yield stress is further reduced. The yield stress increases slowly to 0.82 GPa when L/d=60, and it changes to 0.83 GPa when L/d=72. In the plastic deformation stage, the higher the strain generated by the silver nanowires during the tensile process, the better the flexibility of the silver nanowires. As shown in Fig. 10c, with increasing the aspect ratio of silver nanowires, the yield strain of nanowires fluctuates and reaches a maximum value at the aspect ratio of 60. Fig. 10d shows the relationship between Young's modulus and aspect ratio, which reflects the deformation resistance of the materials. It can be seen that the Young's modulus changes significantly when the aspect ratio of the silver nanowires is relatively low, and it hardly changes when the aspect ratio of the silver nanowires increases to 60.

In the elastic deformation stage, the surface stress exists on the silver nanowires, and the crystal structure is undamaged when the tensile load does not exceed the elastic limit. In the plastic deformation stage, the dislocations can move along the slip direction on the slip surface. The slip process can be blocked by the obstacles, such as precipitation phase and grain boundaries. The dislocations are pinned at the grain boundaries, thereby increasing the dislocation density, causing stress concentration, and producing microcracks[26–27]. Thus, the silver nanowires fracture. The increased aspect ratio of silver nanowires and the increase in the number of grains and grain boundaries result in the shorter distance of dislocation movement. Thus, more dislocation movements are required to achieve the corresponding strain. The Hall-Petch formula[28] can be used to describe the relationship between grain boundaries and yield stress. With increasing the number of grains and decreasing the grain size, the grain boundaries are increased. Therefore, the yield strength is increased with increasing the aspect ratio of silver nanowires.

$$\delta = \delta_0 + kd^{-1/2} \tag{4}$$

where δ is the yield stress of crystal; δ_0 is the critical tensile stress of the starting slip system; k is a constant; d is the grain size.

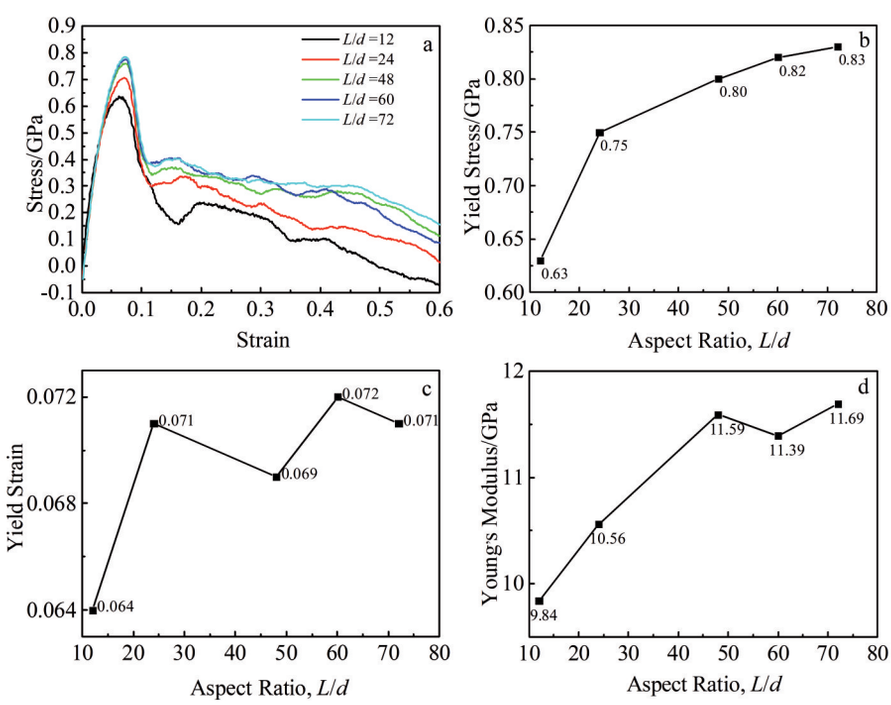

Fig.10 Stress-strain curves of silver nanowires with different aspect ratios (a); relationships of yield stress (b), yield strain (c), and Young's modulus (d) with aspect ratio of silver nanowires

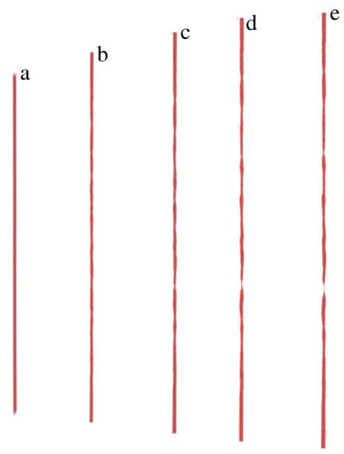

Fig.11 Schematic diagrams of silver nanowires at 0 ps (a), 37 ps (b), 54 ps (c), 90 ps (d), and 100 ps (e) during tensile fracture process

2.2.3 Stretching process at different temperatures

Fig. 12a shows the stress-strain curves of single-crystal silver nanowires with aspect ratio of 72 at different temperatures. It can be seen that the single-crystal silver nanowires stretched at different temperatures firstly undergo the elastic deformation and then suffer the plastic deformation. It can be seen from Fig. 12b that the yield stress of single-crystal silver nanowires is decreased with increasing the temperature. With increasing the temperature from 300 K to 400 K, from 400 K to 500 K, from 500 K to 600 K, and from 600 K to 900 K, the yield stress is decreased by 4.54%, 4.76%, 6.25%, and 17.33%, respectively. According to Fig. 12c, the yield strain is also decreased with increasing the temperature, but the change amplitude is insignificant. Fig. 12d shows that the Young's modulus is firstly increased and then decreased with increasing the temperature and it reaches the maximum value of 11.83 GPa at 400 K.

The yield stress is decreased with increasing the temperature, which can be explained by Eq.(5)[29–30], as follows:

$$\tau_P = \frac{2G}{1-v}\exp\left(-\frac{2\pi\omega}{b}\right) \quad (5)$$

where τ_P is the starting force of dislocation; G is the shear modulus; v is the Poisson ratio; ω is the dislocation width; b is the Park vector. The higher the temperature, the lower the shear modulus. According to Eq. (5), with increasing the temperature, the force required for dislocation initiation is decreased, many dislocations move, and the yield strength of single-crystal silver nanowires is decreased.

2.2.4 Melting process

Fig. 13a shows the relationship between potential energy and temperature of silver nanowires with different aspect ratios during the melting process. It can be seen that there are three abrupt changes in the potential energy during the melting of silver nanowires. The first abrupt change of potential energy occurs at about 670 K, indicating that the silver nanowires break off to form nanoclusters. The second abrupt change of potential energy occurs at about 1030 K, corresponding to the melting temperature of silver nanoparticles with particle size of 20 nm. The third abrupt change of potential energy occurs at about 1256 K, which is close to the melting temperature of block silver and also close to the theoretical temperature for single-crystal silver production during the melting of silver nanowires.

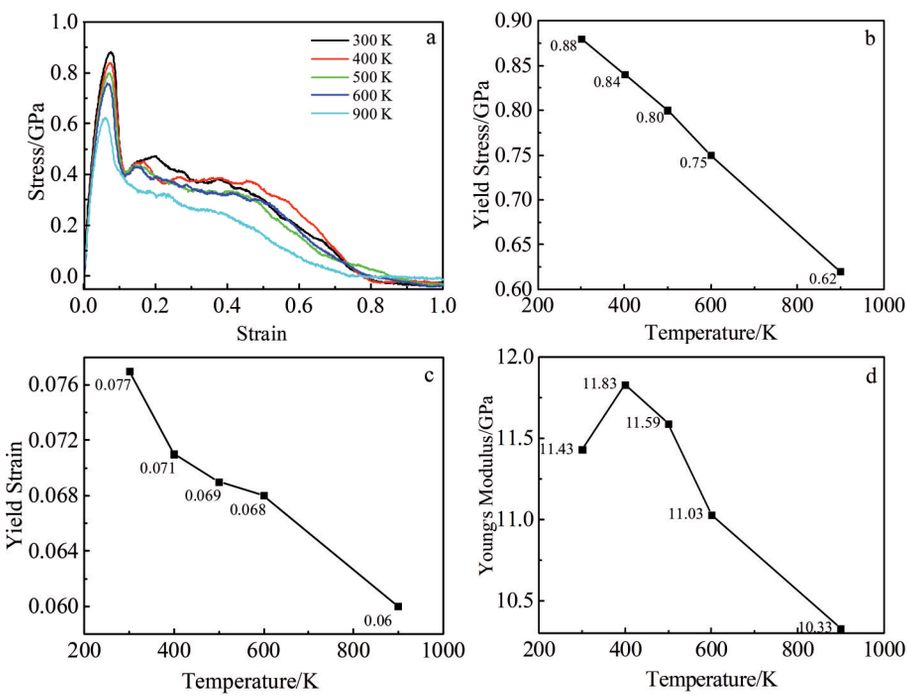

Fig.12 Stress-strain curves of silver nanowires with aspect ratio of 72 at different temperatures (a); relationships of yield stress (b), yield strain (c), and Young's modulus (d) with temperature of silver nanowires

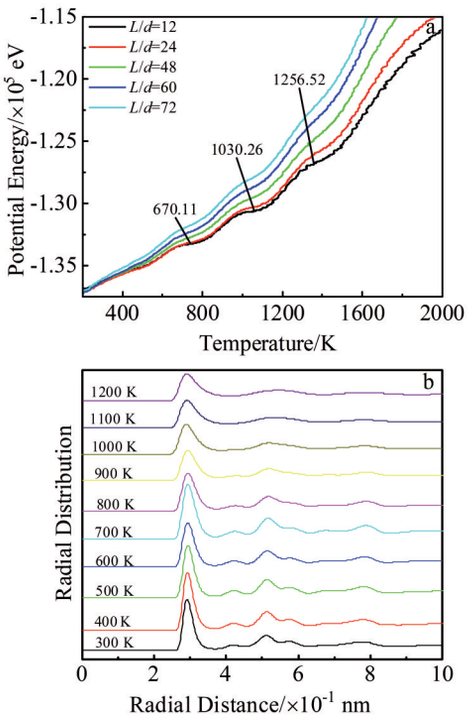

Fig.13 Relationship between potential energy and temperature of silver nanowires with different aspect ratios (a); radial distributions of single-crystal silver nanowires with aspect ratio of 12 at different temperatures (b)

Fig. 13b shows the radial distributions of single-crystal silver nanowires with aspect ratio of 12 at different temperatures, which can reflect the relevant information of the atoms in the system. The peaks are sharp at temperatures of 300, 400, and 500 K, indicating that the silver nanowires have good crystallinity and no fracture occurs. At 600 K, the first peak expands and the peak strength is weakened. Meanwhile, the intensity of peak at radial distance of 0.55 nm becomes weaker, and this peak disappears completely at 700 K, indicating that the size of the silver nanowires becomes larger and the silver nanowires are more disordered. When the temperature increases to 1000 K, each peak becomes significantly broader and their intensity becomes weaker. The second, fourth, and fifth characteristic peaks disappear, indicating that the long-range ordered structure is completely destroyed with increasing the temperature. When the temperature rises to 1200 K, the first characteristic peak is weakened and other peaks can hardly be observed, suggesting that the nanoparticles are transformed from solid phase to liquid phase and the short-range ordered structure is destroyed.

Fig. 14 shows the simulated melting temperatures of silver nanowires with different aspect ratios. It can be seen from Fig. 14 that the melting temperature of silver nanowires is decreased with increasing the aspect ratio, because the bonding energy of the surface atoms of silver nanowires is much smaller than that of the internal atoms. The smaller the ratio of surface area to volume of nanowires with small aspect ratio, the higher the overall melting temperature. The fitting curve in Fig.14 can be expressed by Eq.(6), as follows:

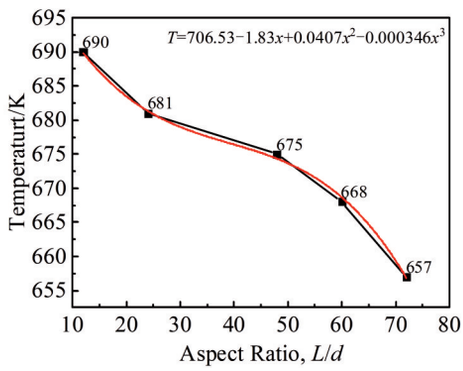

Fig.14 Simulated melting temperatures of silver nanowires with different aspect ratios

Table 2 Comparison of melting temperatures of silver nanowires with different PVP/$AgNO_3$ molar ratios

PVP/$AgNO_3$ molar ratio	Theoretical/K	Experimental/K
1.5	609.39	559.05
3.0	602.93	555.05
4.5	602.85	554.85
6.0	600.01	554.35
7.5	612.35	560.35

$$T = 706.53 - 1.83x + 0.047x^2 - 0.000\,346x^3 \quad (6)$$

where T (K) is the melting temperature; x is the aspect ratio.

The fitting curve agrees well with the theoretical values calculated by simulation. Thus, the melting temperature of the single-crystal silver nanowires is decreased with increasing the aspect ratio. The decreasing rate of melting temperature reaches the minimum when the aspect ratio is 39.2. The melting temperature of silver nanowires with different PVP contents was estimated by Eq. (6), and Table 2 shows the comparison between the experimental results and the theoretical results. According to Table 2, the theoretical melting temperatures are all higher than the experimental ones, because the single-crystal silver nanowires are structurally stable with fixed bond angles and bond lengths. Thus, more energy is required to destroy the ordered arrangement of the atoms during melting process.

3 Conclusions

1) By controlling the polyvinylpyrrolidone (PVP) content, the aspect ratio of silver nanowires can be adjusted. Thus, PVP selectively adsorbs on different crystal planes. PVP with low content cannot passivate all the Ag (100) crystal planes, and the silver nanowires are coarsened. PVP with high content can passivate both the Ag (100) and Ag (111) crystal planes, and the silver nanowires become short. The optimal diameter of 77.7 nm of silver nanowires can be obtained by synthesis at the molar ratio of PVP/$AgNO_3$=6.0.

2) The silver nanowires are composed of face-centered

cubic silver, which has more than two sets of diffraction patterns.

3) With increasing the aspect ratio of silver nanowires, the number of grain boundaries is decreased, and the dislocation movement is hindered. Thus, the dislocation slip becomes complex, the dislocation density decreases, and the stress concentration can hardly appear. As a result, the yield strength of silver nanowires is enhanced.

4) The deformation behavior of silver nanowires is temperature-dependent, and the yield strength of silver nanowires is decreased with increasing the temperature.

5) The melting temperature of single-crystal silver nanowires is decreased with increasing the aspect ratio of silver nanowires, and all theoretical melting temperatures are higher than the experimental ones of silver nanowires.

References

1 Wang C, Cheng B S, Zhang H C *et al. Nano Research*[J], 2016, 9(5): 1532
2 Aurang P, Doganay D, Bek A *et al*. *Solar Energy*[J], 2017, 141: 110
3 Masaharu T, Yuki N, Kisei M *et al*. *Materials Letters*[J], 2006, 60(6): 834
4 Yang R, Sui C H, Gong J *et al*. *Materials Letters*[J], 2007, 61(3): 900
5 Zheng X J, Jiang Z Y, Xie Z X *et al*. *Electrochemistry Communications*[J], 2007, 9(4): 629
6 Liu Y, Chen Y Y, Shi R *et al*. *RSC Advances*[J], 2017, 7(9): 4891
7 Sun Y, Xia Y. *Advanced Materials*[J], 2002, 14(11): 833
8 Yuan X M, Yang H W, Li Y X *et al*. *Langmuir*[J], 2019, 35(36): 11 829
9 Xu S, Guo Y F, Ngan A. *International Journal of Plasticity*[J], 2013, 43: 116
10 Zhang Xiaoyong, Zhang Bing, Li Chao *et al*. *Rare Metal Materials and Engineering*[J], 2013, 42(10): 2057 (in Chinese)
11 Wang J, Li N, Anderoglu O *et al*. *Acta Materialia*[J], 2010, 58(6): 2262
12 Zhao Jianwei, Li Ren, Cheng Na *et al*. *Scientia Sinica Technologica*[J], 2017, 48(2): 143 (in Chinese)
13 Ahluwalia V, Elumalai S, Kumar V *et al*. *Microbial Pathogenesis*[J], 2018, 114: 402
14 Ran Yunxia, He Weiwei, Wang Ke *et al*. *Chemical Communications*[J], 2014, 50(94): 14 877
15 Chi Y, Tu J C, Wang M G *et al*. *Journal of Colloid and Interface Science*[J], 2014, 423: 54
16 Lee H S, Kim Y W, Kim J E *et al*. *Acta Materialia*[J], 2015, 83: 84
17 Andersson M, Pedersen J S, Palmqvist A. *Langmuir*[J], 2005, 21(24): 11 387
18 Clavero C. *Nature Photonics*[J], 2014, 8(2): 95
19 Lee E J, Kim Y H, Hwang D K *et al*. *RSC Advances*[J], 2016, 6(14): 11 702
20 Wang Z H, Liu J W, Chen X Y *et al*. *Chemistry: A European Journal*[J], 2004, 11(1): 160
21 Liu S, Wen Y H, Zhu Z Z. *Chinese Physics B*[J], 2008, 17(7): 2621
22 Wang L, Fang L H, Gong J H. *Transactions of Nonferrous Metals Society of China*[J], 2012, 22(1): 170
23 Fang L H, Wang L, Gong J H *et al*. *Transactions of Nonferrous Metals Society of China*[J], 2010, 20(5): 857
24 Wen Y H, Zhu Z Z, Zhu R Z *et al*. *Physica E: Low-Dimensional Systems and Nanostructures*[J], 2004, 25(1): 47
25 Lei Y W, Sun X R, Zhou R L *et al*. *Computational Materials Science*[J], 2018, 150: 1
26 Kong D L, Xin T J, Sun S D *et al*. *Nano Letters*[J], 2019, 19(1): 292
27 Wang L H, Teng J, Sha X C *et al*. *Nano Letters*[J], 2017, 17(8): 4733
28 Zhao J W, Cheng N, Wang X X *et al*. *Chinese Journal of Inorganic Chemistry*[J], 2018, 34(1): 43
29 Keung W C, Lee Y F, Shan W W *et al*. *Solid State Phenomena*[J], 2008, 141(143): 319
30 Qiu Y, Young M L, Nie X. *Shape Memory and Superelasticity*[J], 2015, 1(3): 310

不同长径比纳米银线合成机理及变形机理

赵梅莉[1]，甘国友[1]，冷崇燕[1]，徐凤仙[1]，袁　鹏[1]，白海龙[2]，吕金梅[3]，严继康[1,4]

(1. 昆明理工大学 材料科学与工程学院，云南 昆明 650093)

(2. 云南锡业集团(控股)有限责任公司 研发中心，云南 昆明 650000)

(3. 云南锡业锡材有限公司，云南 昆明 650501)

(4. 西南石油大学 工程学院，四川 南充 637001)

摘　要：采用液相还原法，通过调节聚乙烯吡咯烷酮（PVP）摩尔浓度制备不同长径比的纳米银线。采用X射线衍射仪、扫描电子显微镜、紫外-可见光分光光度计、同步热分析仪及透射电子显微镜对纳米银线的物相组成、微观形貌、光吸收性能、热分解、晶体结构进行表征，并使用分子动力学模拟单晶纳米银线的拉伸和熔化过程。结果表明：纳米银线主要由面心立方银构成。PVP与$AgNO_3$的摩尔比由1.5变为7.5，纳米银线直径先减小后增加；当摩尔比为6.0时，纳米银线直径最小，为77.7 nm。纳米银线直径由106.1 nm减小为77.7 nm，熔化温度随之减小，最低为281.2 ℃。单晶纳米银线长径比由6变为72时，屈服强度逐渐由0.63 GPa提升至0.83 GPa。单晶纳米银线熔化温度随长径比增加而减小，由690 K变为657 K。PVP与$AgNO_3$的摩尔比为6.0是合成银线的最佳条件，长径比大的纳米银线具有良好的抵抗变形的能力。

关键词：液相还原法；纳米银线；生长机理；分子动力学；长径比

作者简介：赵梅莉，女，1998年生，硕士生，昆明理工大学材料科学与工程学院，云南 昆明 650093，E-mail：1493561656@qq.com